Mechanical Technology and Engineering Insights

www.mtei.reapress.com

Mech. Technol. Eng. Insights . Vol. 2, No. 3 (2025) 199–209.

Paper Type: Original Article

Numerical Analysis of Combined Heat and Mass Transfer by Mixed Convection over a Vertical Wall

Khadijeh Ghaziyani[1,*], Mehdi Moslemi[2]

[1] Department of Mathematics, Ayandegan University, Tonekabon, Iran; Ghaziyani89@gmail.com.
[2] Department of Mechanical Engineering, Ayandegan Institute of Higher Education, Tonekabon, Iran; mehdimoslemi1982@gmail.com.

Citation:

Received: 17 November 2024 *Revised: 18 January 2025* *Accepted: 24 March 2025*	Ghaziyani, Kh. (2025). Numerical analysis of combined heat and mass transfer by mixed convection over a vertical wall. *Mechanical Technology and Engineering Insights, 2*(3), 199-209.

Abstract

In this study, combined (mixed) convection heat and mass transfer within the boundary layer along a corrugated vertical surface is numerically investigated. The governing non-dimensionalized partial differential equations are solved using a fully implicit finite difference scheme, ensuring numerical stability and accuracy. The effects of several key physical parameters, including the buoyancy ratio, Richardson number (Ri), Prandtl number (Pr), and Schmidt number (Sc), on the flow, temperature, and concentration fields are systematically examined.The results reveal that increasing the buoyancy ratio and Richardson number significantly enhances both heat and mass transfer rates due to stronger buoyancy-induced flow. It is also observed that higher Prandtl numbers lead to an increase in the heat transfer rate, indicating thinner thermal boundary layers. Similarly, an increase in the Schmidt number results in enhanced mass transfer, corresponding to reduced concentration boundary layer thickness. Moreover, the influence of the wavy surface geometry on velocity, temperature, and concentration distributions is analyzed, demonstrating that surface corrugation plays an important role in modifying the boundary layer structure and transport characteristics. The outcomes of this study provide useful insights for the optimization and design of high-efficiency heat exchangers, chemical processing devices, and other engineering systems involving mixed convection flow over non-flat or wavy surfaces.

Keywords: Heat and mass transfer, Mixed convection, Boundary layer flow, Vertical surface, Numerical solution, Finite difference method.

1 | Introduction

Given the significance of combined heat transfer accompanied by concentration changes, extensive research has been conducted in this field in recent years. The influence of buoyancy forces, resulting from temperature

Corresponding Author: Ghaziyani89@gmail.comjfea
https://doi.org/10.48313/mtei.v2i3.54
Licensee System Analytics. This article is an open access article distributed under the terms and conditions of the Creative Commons Attribution (CC BY) license (http://creativecommons.org/licenses/by/4.0).

and concentration gradients, plays a crucial role in heat and mass transfer processes. These phenomena are prevalent in numerous physical processes and engineering applications. Key examples include chemical distillation, the formation and dispersion of opacifiers, the design of heat exchangers, solar energy collectors, and thermal protection systems. Therefore, the study of mixed convection heat and mass transfer is of paramount importance. The interaction between flow convection and variations in temperature and concentration has been continuously studied in the past, with various findings reported in the literature. When heat transfer is coupled with mass transfer, the fluid flow exhibits mixed convection characteristics, particularly when free and forced convection mechanisms interact.

Regarding research in the field of heat and mass transfer, Bottemanne [1] investigated steady-state free convection heat and mass transfer along a flat surface. They solved the governing equations analytically for Pr = 0.71 and Sc = 0.63. Callahan and Marner [2] examined free convection heat and mass transfer over a flat surface for $Pr = 1.0$ and a reasonable range of Schmidt numbers. Chang et al. [3] analyzed the effects of buoyancy forces on free heat and mass transfer within an open vertical duct. Yan and Lin [4] studied heat and mass transfer over two parallel plates featuring an evaporation layer. Further investigation into heat and mass transfer between parallel plates was conducted by Yan et al. [5], where they employed numerical methods to solve the equations. Lai [6] explored natural heat and mass transfer in porous media. Additionally, Yan [7] investigated combined heat and mass transfer in the turbulent flow of a wetted channel.

In the present study, the combined heat and mass transfer of a Newtonian fluid along a vertical surface is investigated. After non-dimensionalizing the governing equations, the effects of key parameters such as the buoyancy ratio, Richardson number, Prandtl number, and Schmidt number on the Nusselt number, Sherwood number, and skin friction coefficient are examined. Furthermore, the influence of these parameters on the velocity, temperature, and concentration profiles is thoroughly analyzed. Nervo [8] aims to introduce the fundamentals of numerical methods in heat transfer and fluid dynamics and to apply them to the numerical analysis of a flat-plate solar collector. Jodat et al. [9] the injection of a small amount of micronized ethanol into a natural gas flame was investigated to enhance radiative heat transfer and reduce NOx emissions, and the results showed an increase in radiative heat flux along with a significant reduction in NOx. Aliaga et al. [10] introduces a novel concentrated solar chimney system with a compact design and high thermal efficiency that, by integrating solar concentration, molten salt thermal storage, and CFD modeling, significantly improves performance, response time, and cost-effectiveness compared to conventional systems.

Askari and Taheri [10] in numerical study investigates natural convection heat transfer in a square enclosure with two semi-circular constant heaters using the finite element method. The results show that heater spacing, Hartmann number, and Rayleigh number significantly influence flow structure and heat transfer, governing the transition between conduction- and convection-dominated regimes. In [11] forced convection flow and heat transfer between two parallel plates partially filled with a porous medium using the lattice Boltzmann method. The results show that the presence of square obstacles representing the porous medium enhances thermal performance and increases the average Nusselt number. In the paper [12], the natural convection heat transfer of water-alumina nanofluid in a square porous cavity was investigated using the lattice Boltzmann method, analyzing the effects of Rayleigh and Darcy numbers, porosity, and nanoparticle volume fraction on flow and heat transfer. The results showed that increasing the nanoparticle fraction and Rayleigh number enhances heat transfer, while the porous medium restricts the flow. In the paper [13], the dynamic and thermal behavior of turbulent air flow in a two-dimensional horizontal channel with inclined baffles was numerically investigated. The results showed that increasing the baffle inclination enhances turbulence, alters flow distribution, and improves heat transfer and the local Nusselt number.

vertical plate is investigated. Following the non-dimensionalization of the governing equations, the influence of various parameters, including the buoyancy ratio, Richardson number (Ri), Prandtl number (Pr), and Schmidt number (Sc), on the Nusselt number (Nu), Sherwood number (Sh), and skin friction coefficient (C_f) is examined. Furthermore, the effects of these parameters on the velocity, temperature, and concentration profiles are thoroughly analyzed.

2 | Mathematical Formulation

The boundary layer flow of the fluid under consideration passes over a semi-infinite vertical surface. The corrugated surface of the body is maintained at a constant temperature (T_w) and constant concentration (C_w), which are higher than the ambient temperature (T_\infty) and concentration (C_\infty). The free-stream velocity and the inlet velocity (at the leading edge of the plate) are assumed to be zero. Furthermore, the fluid flow is considered to be laminar, incompressible, steady, and two-dimensional. Viscous dissipation effects are neglected. Accordingly, by employing the boundary layer approximation and the Boussinesq approximation, the governing equations are formulated as follows:

$$\frac{\partial u}{\partial x}+\frac{\partial v}{\partial y}=0. \tag{1}$$

$$u\frac{\partial u}{\partial x}+v\frac{\partial u}{\partial y}=\nu\frac{\partial^2 u}{\partial y^2}+g\beta_T\left(T-T_\infty\right)+g\beta_c\left(c-c_\infty\right). \tag{2}$$

$$u\frac{\partial T}{\partial x}+v\frac{\partial T}{\partial y}=\left(\frac{\nu}{Pr}\right)\frac{\partial^2 T}{\partial y^2}. \tag{3}$$

$$u\frac{\partial c}{\partial x}+v\frac{\partial c}{\partial y}=D\frac{\partial^2 c}{\partial y^2}. \tag{4}$$

The boundary conditions for the governing equations are specified as follows:

I. On the surface (y = 0): $T=T_w, c=C_w, u=v=0.$

II. In the free stream ($y\to\infty$): $T\to T_\infty, c\to C_\infty, u=U_\infty.$

The dimensionless variables are defined as follows:

$$\begin{aligned}
&X=\frac{x}{L}, y=\frac{y\sqrt{Re}}{L}, U=\frac{u}{U_\infty}, V=\frac{v\sqrt{Re}}{U_\infty},\\
&\theta=\frac{T-T_\infty}{T_w-T_\infty}, C=\frac{c-C_\infty}{C_w-C_\infty}, Re=\frac{U_\infty L}{\nu},\\
&Pr=\frac{\mu C_p}{K}, Sc=\frac{\mu}{\rho D}, Ri=\frac{Gr}{Re^2}, N=\frac{\beta_c\left(C_w-C_\infty\right)}{\beta_T\left(T_w-T_\infty\right)},\\
&, Gr=\frac{g\beta_t\left(T_w-T_\infty\right)\rho^2 L^3}{\mu^2}.
\end{aligned} \tag{5}$$

Substituting the dimensionless *Variables (5)* into *Eqs. (1)–(4)* yields the following system of equations for numerical analysis:

$$\frac{\partial U}{\partial X}+\frac{\partial V}{\partial Y}=0. \tag{6}$$

$$U\frac{\partial U}{\partial X}+V\frac{\partial U}{\partial X}=\frac{\partial^2 U}{\partial Y^2}+Ri(\theta+NC). \tag{7}$$

$$U\frac{\partial \theta}{\partial X}+V\frac{\partial \theta}{\partial Y}=\frac{1}{Pr}\left(\frac{\partial^2 \theta}{\partial Y^2}\right). \tag{8}$$

$$U\frac{\partial C}{\partial X}+V\frac{\partial C}{\partial Y}=\frac{1}{Sc}\left(\frac{\partial^2 C}{\partial Y^2}\right). \tag{9}$$

The boundary conditions in the dimensionless form are expressed as follows:

On the surface (y = 0): $\theta=0, C=1, U=V=0.$

In the free stream ($y\to\infty$): $\theta=0, C=0, U=1.$

The local Nusselt number is defined by the following relation:

$$Nu_{\bar{x}} = \frac{hx}{K_f}. \quad \textbf{(10)}$$

By employing Newton's law of cooling and Fourier's law, the local Nusselt number can be expressed as follows:

$$Nu_{\bar{x}} = \frac{\frac{\partial T}{\partial y}\bar{x}}{T_w - T_\infty}. \quad \textbf{(11)}$$

The following expression for the local Nusselt number is obtained after performing the necessary transformations:

$$Nu_{\bar{x}}\, Re_x^{1/2} = \left.\frac{\partial \theta}{\partial y}\right|_{y=0}. \quad \textbf{(12)}$$

The local Sherwood number is defined by the following expression:

$$Sh_x = \frac{h_d \bar{x}}{D} = \frac{\partial c / \partial y\, x}{C_w - C_\infty}. \quad \textbf{(13)}$$

After performing the transformations, the following expression for the local Sherwood number is obtained:

$$Sh_x\, Re_x^{1/2} = \left.\frac{\partial C}{\partial y}\right|_{y=0}. \quad \textbf{(14)}$$

The shear stress at the surface and the skin friction coefficient are expressed by the following relations:

$$\tau_w = \mu\left(\frac{\partial \bar{u}}{\partial \bar{y}} - \frac{\partial \bar{v}}{\partial \bar{x}}\right). \quad \textbf{(15)}$$

$$C_f = \frac{2\tau_w}{\rho U_\infty^{\,2}}. \quad \textbf{(16)}$$

By substituting *Eq. (16)* into *Eq. (17)*, the following expression is obtained in terms of $(2Re_{\bar{x}})^{1/(2)}\, C_f$:

$$(2Re)^{1/2}\, C_f = \left(\frac{\partial u}{\partial y}\right)^n_{y=0}. \quad \textbf{(17)}$$

3 | Numerical Method

The dimensionless governing *Eqs. (7)-(9)* are solved to obtain the velocity (U), temperature (θ), and concentration (C) fields using a fully implicit decoupled finite difference method. Specifically, for the diffusion and transverse convection terms, a central difference scheme is employed, while the axial convection terms are discretized using a backward difference scheme (upwind scheme). The resulting discretized equations are formulated into a tri-diagonal matrix and solved using the Thomas algorithm by applying the specified boundary conditions.

4 | Results and Discussion

Figs. 1-3 illustrate the effect of the buoyancy ratio (N) on the local Nusselt number, local Sherwood number, and skin friction coefficient. It is observed that an increase in the buoyancy ratio (N) leads to an increase in the Nusselt number, Sherwood number, and skin friction coefficient. This indicates that enhancing the buoyancy force N promotes both heat and mass transfer rates. This trend is physically justifiable because the thicknesses of the thermal and concentration boundary layers decrease as the buoyancy parameter increases. Consequently, given the constant surface temperature, the temperature and concentration gradients at the

wall become steeper the concentration gradient also increases. Consequently, the heat and mass transfer rates, which are proportional to the temperature and concentration gradients, are enhanced.

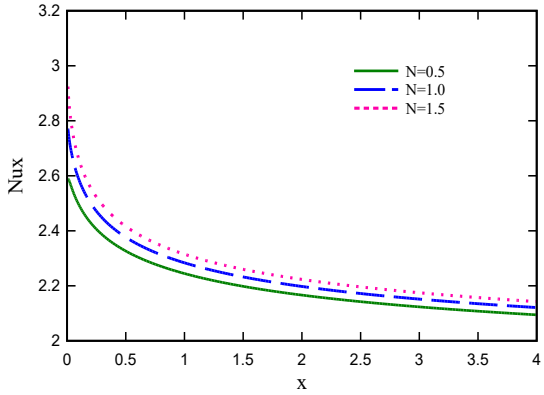

Fig. 1. Axial distribution of the local Nusselt number for Pr = 0.7, Sc = 1.0, Ri = 0.2, and various values of N.

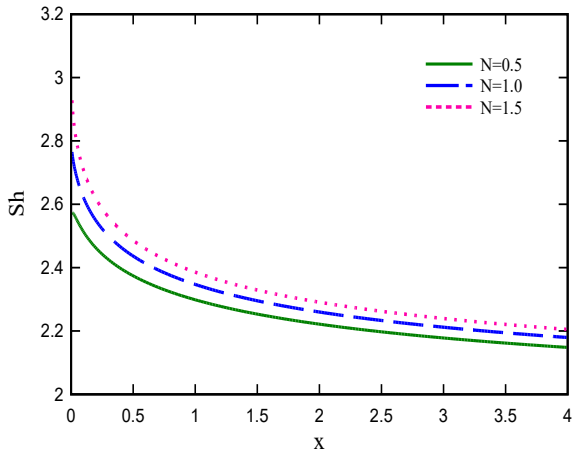

Fig. 2. Axial distribution of the local Sherwood number for Pr = 0.7, Sc = 1.0, Ri = 0.2, and various values of N.

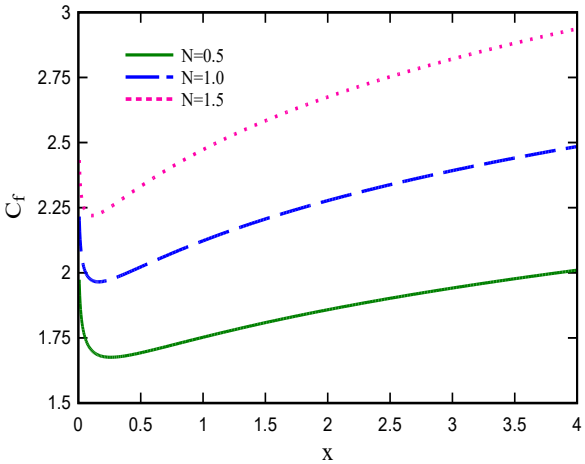

Fig. 3. Axial distribution of the skin friction coefficient for Pr = 0.7, Sc = 1.0, Ri = 0.2, and various values of N.

Figs. 4-6 illustrate the effect of the Richardson number (Ri) on the local Nusselt number, skin friction coefficient, and local Sherwood number, respectively. It is evident that increasing the Richardson number enhances the influence of natural convection, thereby increasing the heat and mass transfer rates. Furthermore, as the buoyancy force intensifies with higher Richardson numbers, the fluid velocity increases, leading to a steeper velocity gradient. Consequently, the skin friction coefficient also increases. The influence of the Richardson number on the velocity profile is depicted in *Fig. 7*.

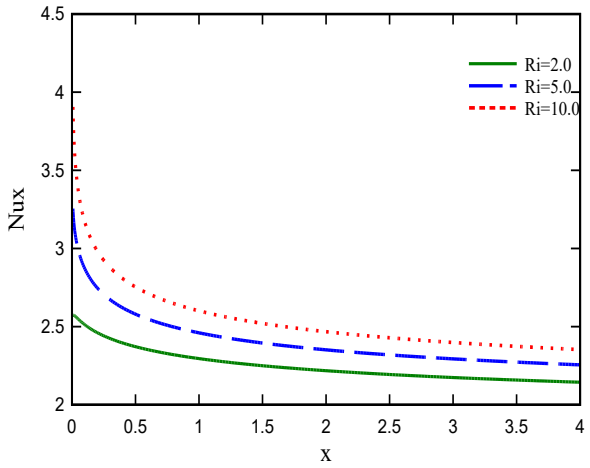

Fig. 4. Axial distribution of the local Nusselt number for Pr = 0.7, Sc = 1.0, N = 1.5, and various values of Ri.

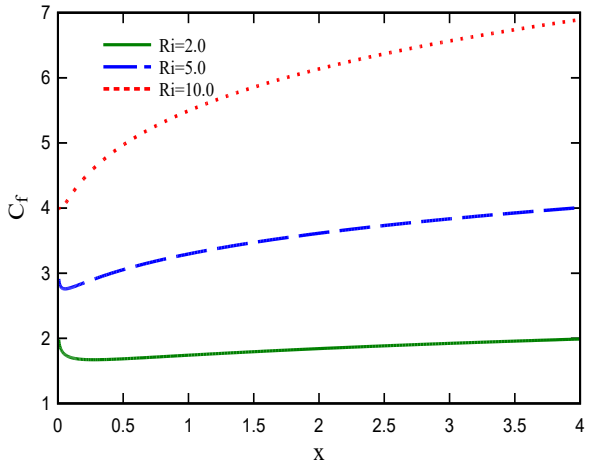

Fig. 5. Axial distribution of the skin friction coefficient for Pr = 0.7, Sc = 1.0, N = 1.5, and various values of Ri.

Fig. 8 and *Fig. 9* illustrate the effect of the Prandtl number (Pr) on the local Nusselt number and skin friction coefficient. It is observed that an increase in the Prandtl number leads to a decrease in the skin friction coefficient. This occurs because lower density enhances the sensitivity of the buoyancy force effect, leading to significant variations in the wall velocity gradient (*Fig. 10*). Conversely, as the Prandtl number increases, the temperature gradient at the wall becomes steeper (*Fig. 11*), resulting in a higher Nusselt number. Furthermore, *Fig. 10* and *Fig. 11* demonstrate that the thermal boundary layer thickness decreases as the Prandtl number increases.

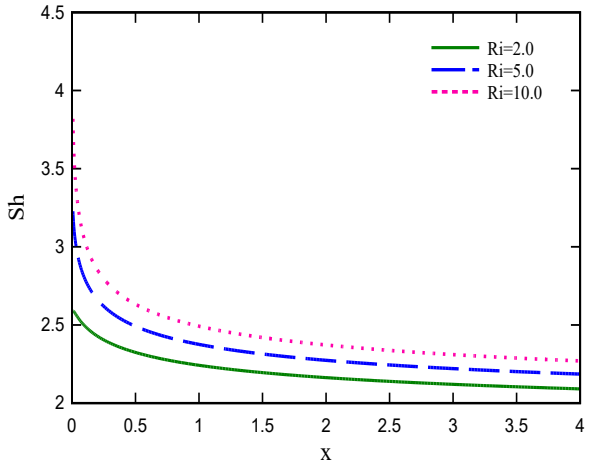

Fig. 6. Axial distribution of the local Sherwood number for Pr = 0.7, Sc = 1.0, N = 1.5, and various values of Ri.

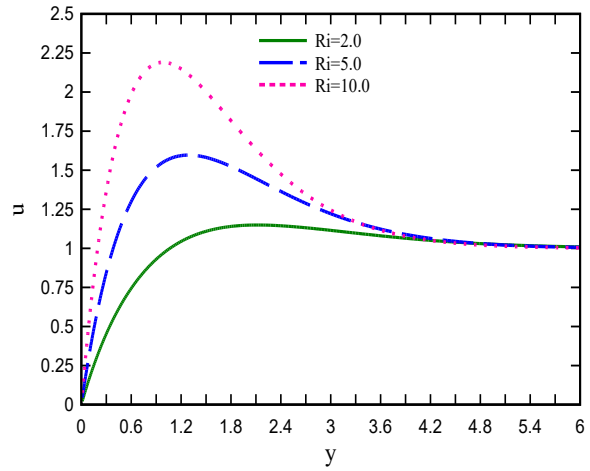

Fig. 7. Temperature profiles for Pr=0.7 ,c=1.0 ,N=1.5 ,and various values of Ri at X=2.5.

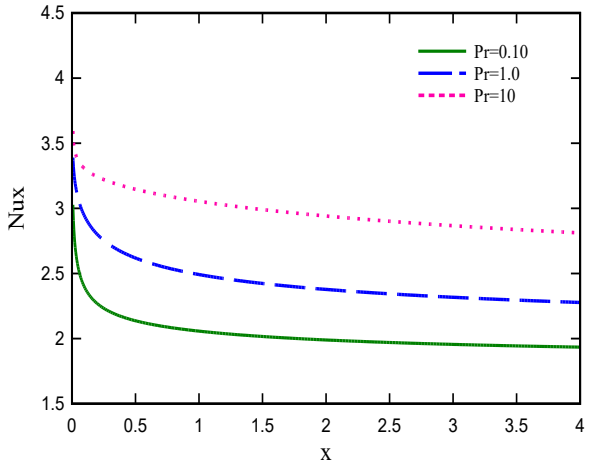

Fig. 8. Axial distribution of the local Nusselt number for $N = 0.75$, $Sc = 0.7$, $Ri = 0.5$, and various Prandtl numbers.

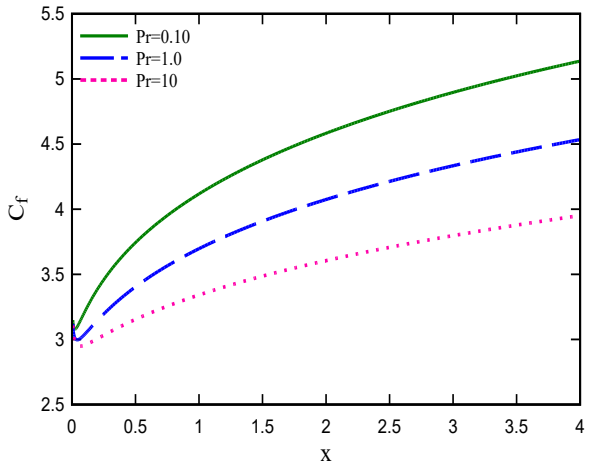

Fig. 9. Axial distribution of the skin friction coefficient for N = 0.75, Sc = 0.7, Ri = 0.5, and various Prandtl numbers.

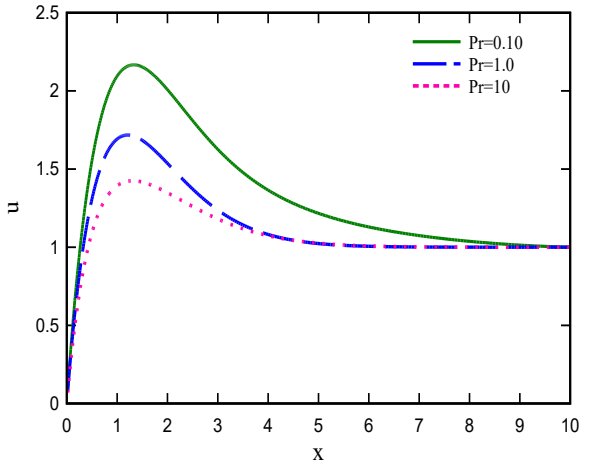

Fig. 10. Velocity profiles for N = 0.75, Ri = 0.5, Sc = 0.7, and various Prandtl numbers at X = 2.5.

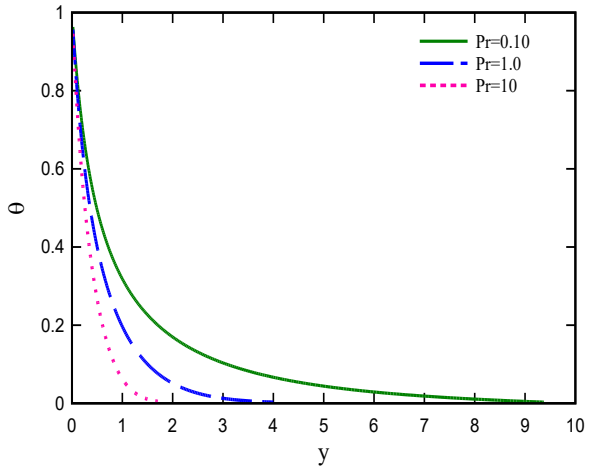

Fig. 11. Temperature profiles for N = 0.75, Ri = 0.5, Sc = 0.7, and various Prandtl numbers at X = 2.5.

Fig. 12 and *Fig. 13* illustrate the influence of the Schmidt number (Sc) on the local Sherwood number and skin friction coefficient. The results indicate that an increase in the Schmidt number leads to an enhancement in the Sherwood number and a reduction in the skin friction coefficient. Since the concentration equation is analogous to the energy equation, the effects of the Schmidt number are expected to be similar to those of the Prandtl number. This can be justified by the fact that an increase in the Schmidt number, which corresponds to a decrease in the mass diffusion coefficient, slows down the fluid motion and enhances the mass transfer rate. Consequently, the concentration gradient at the surface increases, leading to a higher Sherwood number (*Fig. 14*). Furthermore, as the Schmidt number increases, the fluid velocity and its gradient at the wall decrease, resulting in a lower skin friction coefficient. Regarding the concentration profile, it is observed that the thickness of the concentration boundary layer decreases as the Schmidt number increases.

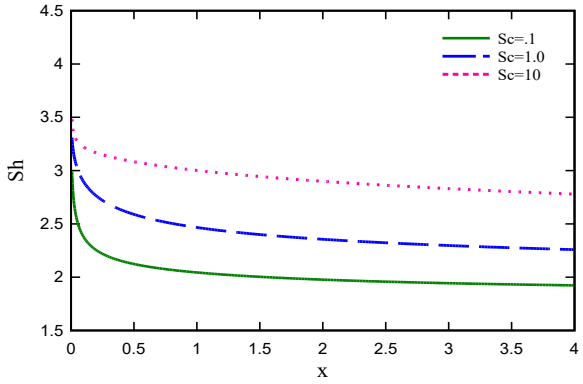

Fig. 12. Axial distribution of the local Sherwood number for N = 0.1, Pr = 0.1, Ri = 0.4, and various Schmidt numbers.

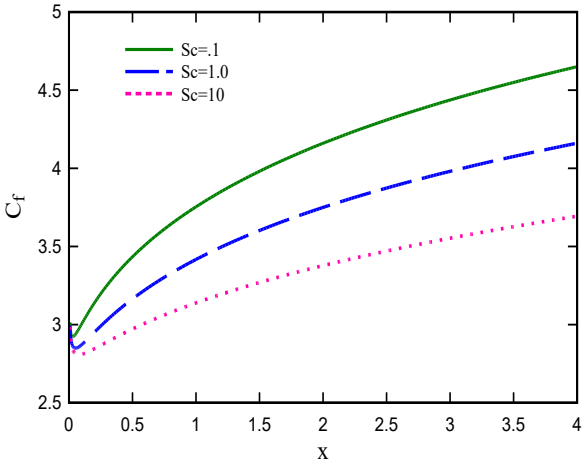

Fig. 13. Axial distribution of the skin friction coefficient for N = 0.1, Pr = 0.1, Ri = 0.4, and various Schmidt numbers.

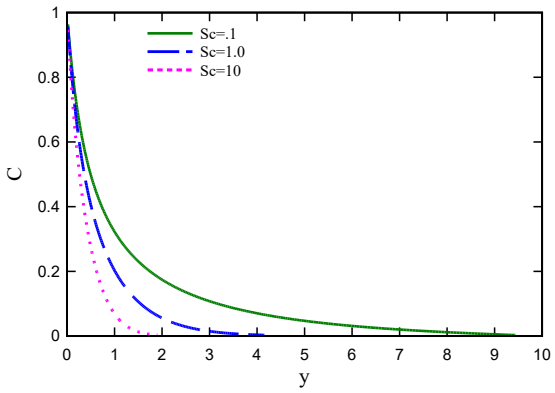

Fig. 14. Concentration profiles for N = 0.1, Pr = 0.1, Ri = 0.4, and various Schmidt numbers at X = 2.5.

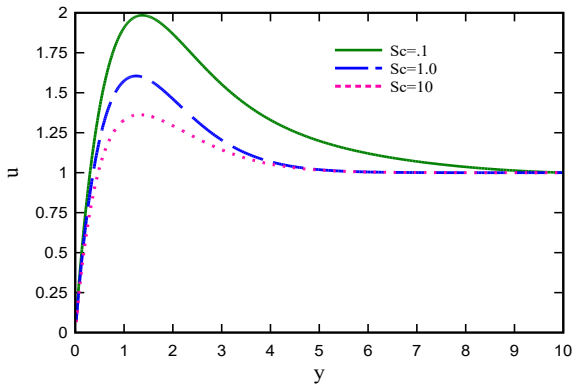

Fig. 15. Velocity profiles for N = 0.1, Pr = 0.1, Ri = 0.4, and various Schmidt numbers at X = 2.5.

5 | Conclusion

In this study, mixed convection heat and mass transfer along a vertical plate has been investigated. The governing equations were non-dimensionalized using appropriate dimensionless parameters and subsequently solved using a fully implicit finite difference method. The key findings are summarized as follows:

An increase in the buoyancy ratio (N) leads to an enhancement in the local Nusselt number, local Sherwood number, and skin friction coefficient.

As the Richardson number (Ri) increases, the influence of natural convection becomes more dominant, resulting in higher heat and mass transfer rates.

The analysis of the Prandtl number (Pr) indicates that higher Pr values lead to a thinner thermal boundary layer, thereby increasing the heat transfer intensity.

Similarly, an increase in the Schmidt number (Sc) results in a higher Sherwood number and a reduction in the concentration boundary layer thickness.

Conflict of Interest

The authors declare that there are no conflicts of interest regarding the publication of this paper.

Data Availability

The datasets generated and/or analyzed during the current study are included in this article.

Funding

This study was carried out without any specific funding from public, commercial, or non-profit organizations.

References

[1] Bottemanne, F. A. (1972). Theoretical solution of simultaneous heat and mass transfer by free convection about a vertical flat plate. *Applied scientific research*, *25*(1), 137–149. https://doi.org/10.1007/BF00382290

[2] Callahan, G. D., & Marner, W. J. (1976). Transient free convection with mass transfer on an isothermal vertical flat plate. *International journal of heat and mass transfer*, *19*(2), 165–174. https://doi.org/10.1016/0017-9310(76)90109-5

[3] Chang, C. J., Lin, T. F., & Yan, W. M. (1986). Natural convection flows in a vertical, open tube resulting from combined buoyancy effects of thermal and mass diffusion. *International journal of heat and mass transfer*, *29*(10), 1543–1552. https://doi.org/10.1016/0017-9310(86)90069-4

[4] Van, W. M., & Lin, T. F. (1990). Combined heat and mass transfer in natural convection between vertical parallel plates with film evaporation. *International journal of heat and mass transfer*, *33*(3), 529–541. https://doi.org/10.1016/0017-9310(90)90187-Y

[5] Yan, W. M., Tsay, Y. L., & Lin, T. F. (1989). Simultaneous heat and mass transfer in laminar mixed convection flows between vertical parallel plates with asymmetric heating. *International journal of heat and fluid flow*, *10*(3), 262–269. https://doi.org/10.1016/0142-727X(89)90045-3

[6] Lai, F. C. (1991). Coupled heat and mass transfer by mixed convection from a vertical plate in a saturated porous medium. *International communications in heat and mass transfer*, *18*(1), 93–106. https://doi.org/10.1016/0735-1933(91)90011-R

[7] Yan, W.-M. (1995). Turbulent mixed convection heat and mass transfer in a wetted channel. *ASME journal of heat and mass transfer*, *117*(1), 229–233. https://doi.org/10.1115/1.2822311

[8] Nervo, E. (2020). Numerical simulations of heat and mass transfer phenomena applied to flat-plate solar collectors [Thesis]. https://webthesis.biblio.polito.it/16223/

[9] Jodat, A., Kameli, A., Najafian, M., & Mahian, O. (2024). Experimental study of nebulized ethanol injection in radiative heat transfer and NOX pollutant of natural gas flame. *Fuel and combustion*, *16*(4), 16-27. (**In Persian**). https://doi.org/10.22034/jfnc.2024.450522.1377

[10] Aliaga, D. M., Feick, R., Brooks, W. K., Mery, M., Gers, R., Levi, J. F., & Romero, C. P. (2021). Modified solar chimney configuration with a heat exchanger: Experiment and CFD simulation. *Thermal science and engineering progress*, *22*, 100850. https://doi.org/10.1016/j.tsep.2021.100850

[11] Askari, N., & Taheri, M. H. (2020). Numerical investigation of a MHD natural convection heat transfer flow in a square enclosure with two heaters on the bottom wall. *Karafan journal*, *17*(1), 97-114. (**In Persian**). https://doi.org/10.48301/kssa.2020.112759

[12] Kayhani, M. H., & Mohebbi, R. (2013). Numerical investigation of fluid flow and heat transfer on the porous media between two parallel plates using the lattice boltzmann method. *Aerospace mechanics*, *9*(1), 63-76. (**In Persian**). https://dor.isc.ac/dor/20.1001.1.26455323.1392.9.1.7.2

[13] Salhi, J. E., Amghar, K., Bouali, H., & Salhi, N. (2020). Combined heat and mass transfer of fluid flowing through horizontal channel by turbulent forced convection. *Modelling and simulation in engineering*, *2020*(1), 1453893. https://doi.org/10.1155/2020/1453893